

Accepted Manuscript

Electroluminescence and photoluminescence of type-II InAs/InAsSb strained-layer superlattices in the mid-infrared

J.A. Keen, E. Repiso, Q. Lu, M. Kesaria, A. R. J. Marshall, A. Krier

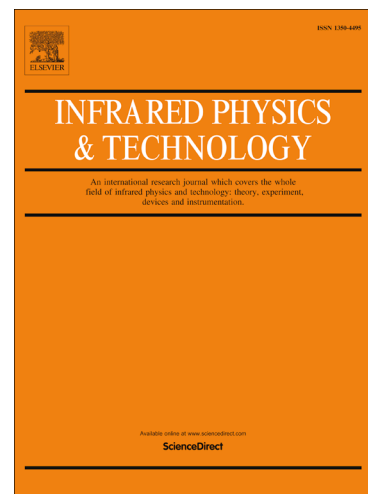
PII: S1350-4495(18)30356-6
DOI: <https://doi.org/10.1016/j.infrared.2018.08.001>
Reference: INFPHY 2654

To appear in: *Infrared Physics & Technology*

Received Date: 25 May 2018
Revised Date: 31 July 2018
Accepted Date: 1 August 2018

Please cite this article as: J.A. Keen, E. Repiso, Q. Lu, M. Kesaria, A. R. J. Marshall, A. Krier, Electroluminescence and photoluminescence of type-II InAs/InAsSb strained-layer superlattices in the mid-infrared, *Infrared Physics & Technology* (2018), doi: <https://doi.org/10.1016/j.infrared.2018.08.001>

This is a PDF file of an unedited manuscript that has been accepted for publication. As a service to our customers we are providing this early version of the manuscript. The manuscript will undergo copyediting, typesetting, and review of the resulting proof before it is published in its final form. Please note that during the production process errors may be discovered which could affect the content, and all legal disclaimers that apply to the journal pertain.



Electroluminescence and photoluminescence of type-II InAs/InAsSb strained-layer superlattices in the mid-infrared

J. A. Keen^{1*}, E. Repiso¹, Q. Lu¹, M. Kesaria², A. R. J. Marshall¹, A. Krier¹

¹ Physics Department, Lancaster University, Lancaster, LA1 4YB, UK

² School of Physics and Astronomy, Cardiff University, Cardiff, CF24 3AA, UK

*j.keen@lancaster.ac.uk

Abstract

There is continuing interest in the development of superlattices for use in photonic devices operating in the technologically important mid-infrared spectral range. In this work type-II strained-layer superlattices of InAs / InAs_{1-x}Sb_x (x=0.04 and x=0.06) were grown on InAs (100) substrates by MBE. Structural analysis of the samples revealed good crystalline quality but a non-uniform distribution of Sb within the QWs which originated from segregation effects during growth. Bright photoluminescence emission was obtained at low temperature (4 K) which persisted up to 300 K. Two prototype samples were grown containing the corresponding superlattices in the active region and fabricated into LEDs. Mid-infrared electroluminescence was obtained from both these LEDs over the temperature range 7 – 300 K and both devices exhibit emission coincident with the main CO₂ absorption band near 4.2 μm at room temperature. These LEDs produced output powers of 8.2 μW and 3.3 μW under 100 mA injection current at room temperature and are of interest for CO₂ detection and further development for mid-infrared gas sensing applications.

Introduction

Light-emitting diodes (LEDs) operating in the technologically important mid-infrared spectral range are highly desirable as key components in instrumentation for a variety of applications, including the sensing and monitoring of environmentally harmful gases, [1, 2, 3], medical diagnostics and treatments [4, 5], space technology [6] and security and defence [7, 8]. However, mid-infrared LED efficiency at room temperature is still quite low and remains hindered by high rates of detrimental non-radiative Auger recombination processes which increase rapidly with injected carrier concentration and emission wavelength [9]. Although there has been extensive research and development of mid-infrared coherent sources such that cascade lasers have now become readily available [10, 11], they require temperature stabilization and are specialist items making them expensive and unsuitable for many of the abovementioned applications. By comparison there has been much less development of incoherent mid-infrared sources. Whilst these now cover the required spectral range most of the existing mid-infrared LEDs are still based on bulk heterostructures of ternary or quaternary III-V alloys [12, 13, 14, 15, 16, 17] and as a result these are limited in efficiency and output power by competing non-

radiative Auger recombination mechanisms. To date there have been few reports of mid-infrared quantum well LEDs [18, 19, 3, 20, 21] and despite their design flexibility, hardly any concerning mid-infrared superlattices being used in the active region [22, 19]. Previously, we reported [23] on the photoluminescence and band structure simulations of InAs / InAsSb multiple quantum well (MQW) and strained-layer superlattice (SLS) structures on InAs substrates, demonstrating their potential for incorporation within mid-infrared LEDs. In this work we report on InAs / InAsSb SLS structures incorporated into mid-infrared LEDs which emit within the spectral range near 4.2 μm and present analysis of their performance characteristics.

Experimental procedures

Two InAs / InAsSb SLS LEDs were grown on n-type ($2 \times 10^{18} \text{ cm}^{-3}$) InAs (100) substrates, 500 μm in thickness, using a VG-V80H MBE system. The active regions of the diodes are based on the InAs / InAsSb SLS structures in our previously reported work [23]. A thermal effusion K-cell provided the In flux, and valved cracker cells provided the group-V As and Sb fluxes. During growth in-situ reflection high energy electron diffraction (RHEED) was used to monitor surface construction. Firstly, a 1.25 μm n-type (Te doped, $1 \times 10^{18} \text{ cm}^{-3}$) InAs layer was grown. Then the undoped active region consisting of a 50-period InAs / InAsSb SLS (total thickness 1.4 μm) was grown. The InAs barrier and InAsSb quantum well thicknesses were 14 nm each, and the Sb content was 4 % and 6 % in samples SLS 1 and SLS 2 respectively. The antimony content of the InAsSb layers was adjusted by changing the temperature of the Sb cell to change the Sb flux. Finally, a 1.25 μm p-type (Be doped, $1.5 \times 10^{17} \text{ cm}^{-3}$) InAs layer was grown to form the p region. The p-n⁰-n diodes were processed in a class 1000 Cleanroom into 800 μm diameter mesa-etched LEDs using conventional photolithography and wet etching processing techniques. Ohmic contacts were provided using Ti (20nm) / Au (200 nm) metallization by thermal evaporation. The chips were mounted onto TO-46 headers for characterization. Figure 1 shows a) schematic of the LED device structure and b) a microscope image showing the mesa etched device and the top contact.

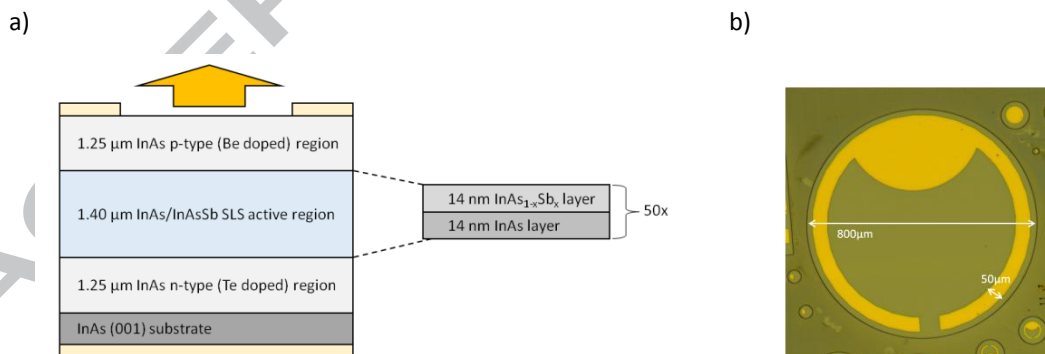


Figure 1 – a) Schematic of the LED structure containing the InAs / InAsSb SLS active region. Samples for PL study were the SLS active region on the substrate without the n/p-doped regions or metal contacts. b) Microscope image showing the mesa etched device and the top contact.

The SLS samples were characterised by high resolution x-ray diffraction (XRD) using a Bede QC 200 system to obtain $\omega - 2\theta$ scans and matched to modelling in Bede Mercury RADS software to determine layer thicknesses and compositions. Transmission electron microscope (TEM) images were acquired from a JEOL 2100 LaB6 TEM system operating at 200 kV. The samples were prepared using standard techniques of grinding / polishing and Ar⁺ ion milling. The final thinning process was undertaken during cooling by liquid nitrogen and with low Ar⁺ ion energies (1 keV) used to minimise surface damage. In the dark field (002) images (Fig. 3) the contrast is proportional to the difference in the mean group III and group V atomic numbers, i.e. the InAs layers are bright and the InAsSb layers are dark.

Electroluminescence was generated from the LEDs using a quasi-continuous injection current of 100 mA (with a duty cycle of 50%) at 1 kHz. The devices were held inside an Oxford Instruments continuous flow cryostat capable of maintaining the LED at a fixed temperature specified in the range 7 - 300 K. The EL emission spectra were recorded using a Bruker Vertex 70 Fourier transform infrared (FTIR) spectrometer in step-scan mode and a 77 K InSb photodetector. For photoluminescence (PL) measurements the same detection system was used but a diode laser (785 nm) was used to excite (2.5 Wcm^{-2}) samples with an identical superlattice but without any p or n cladding layers or metallic contacts.

Results and discussion

The $\omega - 2\theta$ XRD spectra of the two SLS samples, along with theoretical simulations using RADS Mercury software, are shown in Figure 2. The InAs barrier and InAsSb quantum well thickness were each obtained as 14 nm, and the Sb content was determined to be 4 % and 6 % respectively, in agreement with the target design. Strong, well-resolved Pendellosung fringes are evidence of good structural layer quality and abrupt growth interfaces. The average FWHM of the XRD peaks is 171 arcsec for SLS 1 (Sb 4 %) and 303 arcsec in SLS 2 (Sb 6 %) corresponding to more Sb segregation facilitated by the higher strain.

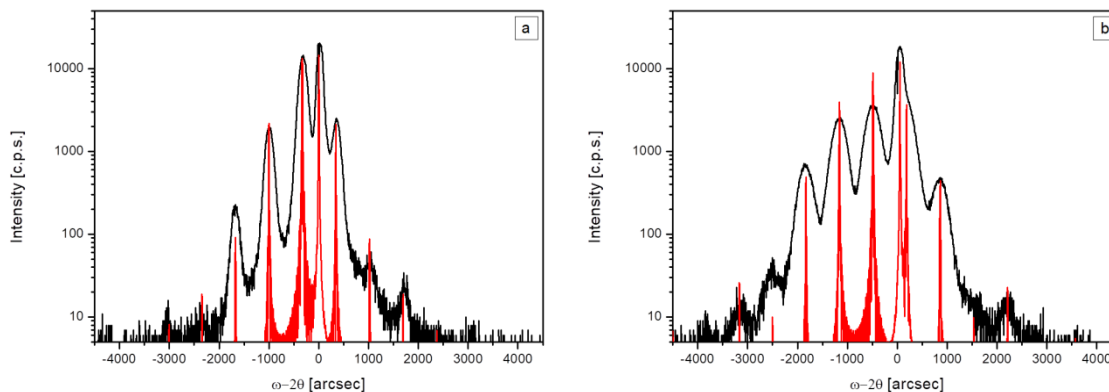


Figure 2 – XRD scans and corresponding simulations to determine the structure and composition of the two SLS samples: (a) SLS 1 and (b) SLS 2 incorporated into the LEDs. Black line – XRD data, red line – XRD model.

According to Mathews and Blakeslee [24] the present samples do not contain sufficient Sb to exceed the critical layer thickness for the creation of dislocations. TEM images from one of the InAs / InAsSb structures (SLS 2) are shown in Figure 3. Although a few threading dislocations are observed at the substrate – SLS interface, and a small number of misfit dislocations can be seen inside the SLS, TEM images taken in different places show defect free regions (although note that TEM analysis here only examines $\sim 10^{-7} \text{cm}^2$). The average layer thicknesses were measured for SLS1 as 12.1 nm for the InAs layers and 15.8 nm for the InAsSb layers, and for SLS2 average thicknesses of 13.2 nm and 13.7 nm, which are a little different from the 14 nm / 14 nm intended design.

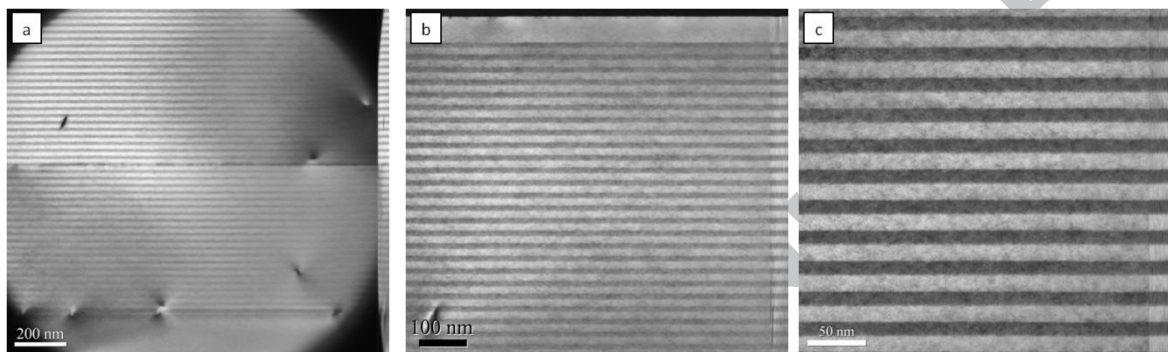
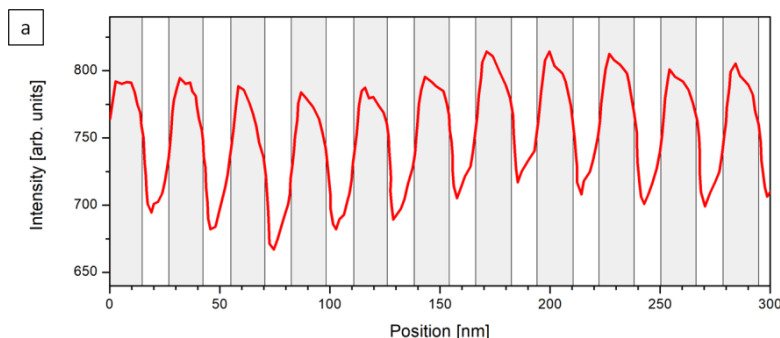


Figure 3 – TEM images (002 dark field) of sample SLS 2 at (a) 200 nm, (b) 100nm and (c) 50 nm resolutions, showing overall good quality structure but with some threading and misfit dislocations present. The contrast is proportional to the difference in the mean group III and group V atomic numbers, i.e. the InAs layers are bright and the InAsSb layers are dark.

To obtain further information about the superlattices, TEM intensity profiles were carried out which are shown in Fig. 4. The profiles of both samples are noticeably asymmetric although the sample SLS 2 with the higher antimony content shows a squarer profile. The shape is consistent with antimony segregation occurring during growth, as described by the Muraki model [25]. The bowing of the intensity profiles is an artefact of the TEM probe beam and does not have an appreciable effect on the shape of the intensity profiles or thickness measurements.



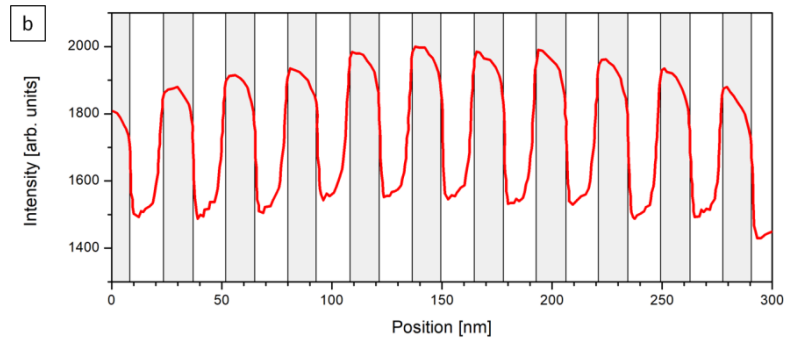


Figure 4 – TEM intensity profile scans showing the Sb concentration profile of (a) SLS 1 (4 % Sb) and (b) SLS 2 (6 % Sb). Measured Sb intensity (red line) and shaded regions indicating the different layers of the superlattice (white – InAs, grey – InAsSb).

Interpretation of the photoluminescence and electroluminescence emission spectra is supported by simulation results produced using *Nextnano* [26]. Figure 5 shows the simulated 4 K band structure and the distribution of the electron and hole wavefunctions within the SLS 1 structure. The effect on these parameters of changing the layer thicknesses and antimony content in the QWs is discussed in more detail in our previous work [23].

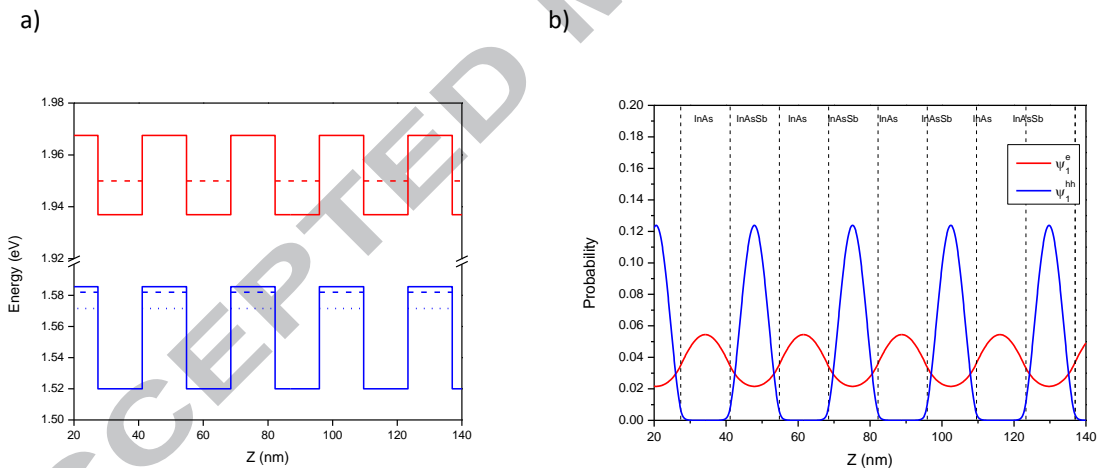


Figure 5 – a) Simulated 4 K band structure of the SLS 1 sample, showing the conduction band (red line), e_1 energy level (red dashed line), valence band (blue line), and the hh_1 and hh_2 energy levels (blue dashed and dotted lines). b) Simulation of electron and hole wavefunction probabilities within the SLS 1 sample, showing strong confinement of the holes inside the InAsSb layers and the tunnelling of the electrons to produce a high proportion of wavefunction overlap.

Electroluminescence emission spectra from the two SLS LEDs at temperatures in the range 7 – 300 K, driven using a constant 100 mA quasi-continuous (qCW) excitation at 1 kHz, are shown in Figure 6, alongside the 4 – 300 K photoluminescence spectra of the corresponding samples as reported in our previous work [23]. In each case the main peak is attributed to recombination between the lowest energy minibands (e_1 - hh_1).

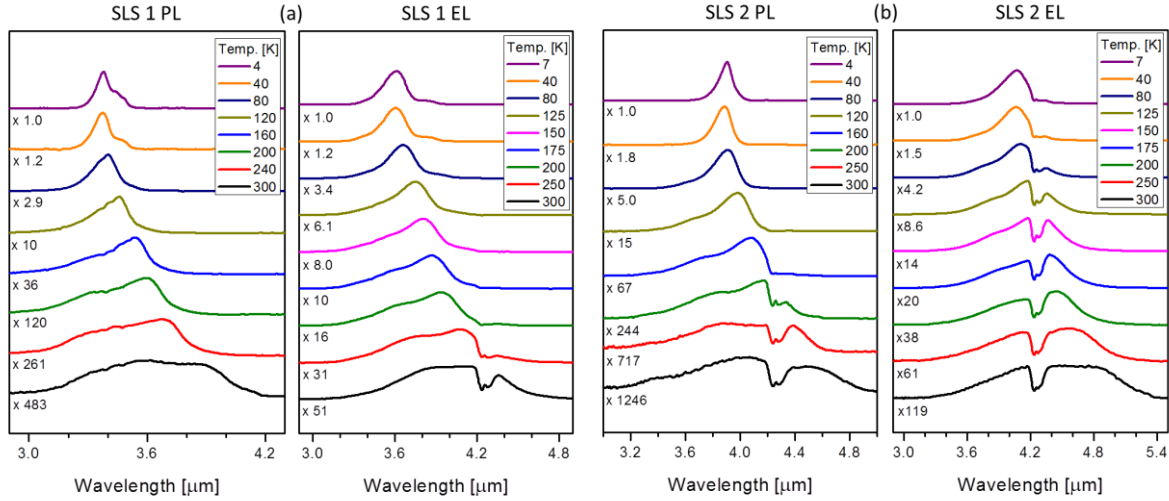


Figure 6 – Normalised (4 – 300 K) photoluminescence spectra of the samples (a) SLS 1 and (b) SLS 2, alongside normalised (7 – 300 K) electroluminescence spectra of the corresponding LEDs.

The CO_2 absorption at 4.2 μm is clearly evident in both the 300 K EL spectra of the LEDs, indicating their potential for use in optical gas detection. Both PL and EL spectra exhibit a redshift in the emission wavelength, spectral broadening, and significant quenching with increasing temperature.

The temperature quenching of the two PL spectra is similar, with a slightly higher rate in the SLS 2 sample containing the higher antimony content (x1246 magnification at 300K compared to x483 for SLS 1). Comparing the two EL spectra, there is a larger decrease in intensity with temperature observed for the SLS 2 LED (x119 magnification at 300K compared to x51 for SLS 1 LED) which has the higher Sb content in the active region. This quenching behaviour originates from the increased type-II band offset which reduces the electron – hole wavefunction overlap and the matrix element for radiative recombination. Simulations using *Nextnano* [26], assuming constant antimony content, a square potential profile and periodic boundary conditions, confirm that with increased antimony content in the InAsSb QWs the structure becomes more type II, increasing both the conduction band and valence band offsets, resulting in greater confinement of the electrons in the InAs layers and of the holes in the QWs. This reduces the overlap of the electron and hole wavefunctions, lowering the recombination rate, and producing a higher density of free carriers (n). Radiative recombination scales as n^2 but the temperature dependent non-radiative Auger recombination processes scale as n^3 , causing larger temperature quenching to occur in the PL and EL of the higher antimony SLS sample and LED respectively. The significantly higher carrier concentration in the EL setup makes the difference in quenching between the two

LEDs more noticeable than between the two SLS samples (1.11 % difference compared to 0.13 %). The higher magnitude of quenching of PL compared to EL is attributed to non-radiative recombination of the carriers near the surface of the SLS samples which have an exposed active region. Simulation results indicate the broad emission spectra at room temperature (300 K) involve additional transitions into confined hole states.

The low temperature (4 K) photoluminescence spectra from the two SLS samples and the corresponding (7 K) electroluminescence spectra from the SLS LEDs are compared in Figs. 7(a) and 7(b). The 4 K PL peaks are identified at 3.38 μm and 3.90 μm , while the wider EL peaks are identified at 3.61 μm and 4.07 μm respectively. In both cases, the EL spectra are red-shifted to longer wavelength compared to the PL spectra. Joule heating can account for some of this peak shift as the series resistance of these diodes was ~ 2.5 Ohms, but we also suppose that this difference originates from the asymmetric distribution of the Sb in the superlattices shown in Fig. 4, such that the depletion layer field in the LED results in a bias dependent shift in the electroluminescence spectra. Similarly, the 300 K PL and EL spectra are shown together in Figs. 7(c) and 7(d). The PL peaks are identified at 3.9 μm and 4.2 μm , with the EL emission of the corresponding LEDs being peaking at 4.4 μm and 4.7 μm . The linewidth of these 300 K spectra are broad, and *Nextnano* simulations of the SLS band structure reveal that up to three heavy hole states contribute to the emission near room temperature. However, there was no evidence of radiative recombination in the InAs barriers associated with hole leakage as we previously observed [23]. Z-plots (not shown) of the emission intensity versus power for the two LEDs at 300 K produce values of $z \approx 2.3$ for both devices, indicating the majority of electron – hole recombination is radiative with no significant compromise to device performance from non-radiative Auger processes (previously we reported [23] Auger suppression in the SLS samples which was expected to also be exhibited from LED devices containing the SLS as the active region).

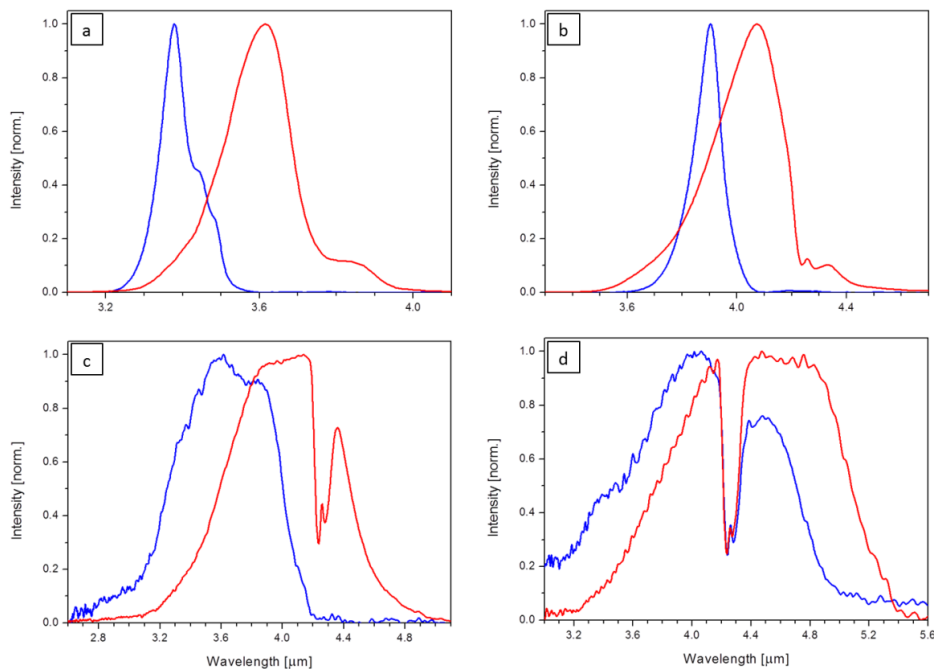


Figure 7 – Comparison of low temperature photoluminescence (4 K) and electroluminescence (7 K) spectra for the two SLS samples (a) SLS 1 and (b) SLS 2. Photoluminescence and electroluminescence (300K) spectra are shown in (c) and (d). Blue curves are PL and red curves are EL.

Output power of the LEDs was measured as 8.2 μW for SLS 1 and 3.3 μW for SLS 2, corresponding to an emittance of 2.13 and 0.86 mW/cm^2 , using a 100 mA quasi-CW injection current at 300 K. Internal quantum efficiencies (IQE) were calculated as 1.95 and 0.84 % respectively. These are similar to IQE values reported for InAs/InAsSb MQW LEDs emitting at similar wavelengths of 2.8 % [19], 2.2% [3] and 0.2 % [21], and of 0.4 % for InSb / InAs QD LEDs [27]. Improvements to the performance could be achieved by inclusion of an electron blocking layer. In similar structures it has been shown that an AlSb barrier (placed at the interface between the p-region and the active region) prevents a large proportion of the carriers escaping from the active region or undergoing non-radiative recombination at this interface, which has been reported to increase the IQE at 300 K typically by a factor of four [19, 22].

Conclusion

Type-II strained layer superlattices of InAs / InAs_{1-x}Sb_x ($x=0.04$ and $x=0.06$) were grown on (100) InAs substrates by MBE. Structural analysis of the samples reveals very good crystalline quality but with a non-uniform distribution of Sb within the QWs which originates from segregation effects during growth. Bright PL emission was obtained at low temperature (4 K) which persisted up to 300 K, although significant thermal quenching was observed. Two p-n⁰-n diode samples were grown containing the corresponding superlattices in the active region and fabricated into LEDs. Mid-infrared electroluminescence was obtained from both these samples over the temperature range 7 – 300 K and both LEDs exhibit emission coincident with the main CO₂ absorption band near 4.2 μm at room temperature. Temperature quenching was observed in both PL and EL spectra, in both

cases being more significant in the structures with higher antimony content in the QWs, which is attributed to the reduced electron – hole wavefunction overlap meaning a higher concentration of free carriers which then recombine non-radiatively by Auger processes. Simulation results indicate the broad emission spectra at room temperature involve e-h recombination from additional confined hole states. These prototype LEDs produced output powers of 8.2 μW and 3.3 μW at 100 mA injection current at room temperature with IQE of $\approx 2\%$ and $\approx 1\%$ respectively. The EL and PL spectra exhibit a redshift in wavelength and spectral broadening, as well as significant quenching with increasing temperature. Since strained layer superlattices offer additional freedom in design it is of interest to further develop LED structures based on our findings for mid-infrared applications.

Acknowledgements

We gratefully acknowledge financial support for this work from EPSRC (EP/J015849/1) and for providing a studentship for J. Keen. This work was also part funded by the EU Marie Skłodowska-Curie Initial Training Network (ITN) PROMIS - Grant agreement No 641899. We wish to thank R. Beanland and A. Sanchez of Integrity Scientific for the TEM analysis of the samples. All data created during this research are openly available from Lancaster University data archive at (<https://doi.org/10.0.68.227/lancaster/researchdata/221>).

References

- [1] D. A. Bui and P. C. Hauser, "Analytical devices based on light-emitting diodes - a review of the state-of-the-art," *Analytica Chimica Acta*, vol. 853, pp. 46-58, 2015.
- [2] M. Kohring, S. Bottger, U. Willer and W. Schade, "LED absorption QEPAS sensor for biogas plants," *Sensors*, vol. 15, no. 5, pp. 12092-12102, 2015.
- [3] P. J. Carrington, Q. Zhuang, M. Yin and A. Krier, "Temperature dependence of mid-infrared electroluminescence in type II InAsSb/InAs multi-quantum well light-emitting diodes," *Semiconductor Science and Technology*, vol. 24, no. 7, p. 075001, 2009.
- [4] S. R. Tsai and M. R. Hamblin, "Biological effects and medical applications of infrared radiation," *Journal of Photochemistry & Photobiology, B: Biology*, vol. 170, pp. 197-207, 2017.
- [5] L. Fleming, D. Gibson, S. G. Song, C. Li and S. Reid, "Reducing N₂O induced cross-talk in a NDIR CO₂ gas sensor for breath analysis using multilayer thin film optical interference coatings," *Surface & Coatings Technology*, vol. 336, pp. 9-16, 2018.
- [6] M. S. Villar, "Mid-infrared absorption spectrometer for multi-species detection using LEDs for space applications: Development and flight testing," University of Central Florida, 2015.
- [7] D. Jung, S. Bank, M. L. Lee and D. Wasserman, "NExt-generation mid-infrared sources," *Journal of Optics*, vol. 19, no. 12, 2017.
- [8] D. T. Norton, J. T. Olesberg, R. T. McGee, N. A. Waite, J. Dickason, K. W. Goossen, J. Lawler, G. Sullivan, A. Ikhlassi, F. Kaimilev, E. J. Koerperick, L. M. Murray, J. P. Prineas and T. F. Boggess, "512 x 512 individually addressable MWIR LED arrays based on type-II InAs/GaSb superlattices," *IEEE Journal Quantum Electronics*, vol. 49, no. 9, 2013.
- [9] A. Krier, *Mid-infrared Semiconductor Optoelectronics*, Springer, 2007.
- [10] M. S. Vitiello, G. Scalari, B. Williams and P. De Natale, "Quantum cascade lasers: 20 years of challenges," *Optics Express*, vol. 23, no. 4, pp. 5167-5182, 2015.
- [11] F. Capasso, "High-performance midinfrared quantum cascade lasers," *Optical Engineering*, vol. 49, no. 11, p. 111102, 2010.
- [12] K. D. Mynbaev, N. L. Bazhenov, A. A. Semakova, A. V. Chernyaev, S. S. Kizhaev, N. D. Stoyanov, V. E.

- Bougrov, H. Lipsanen and K. M. Salikhov, "Spontaneous and stimulated emission in InAsSb-based LED heterostructures," *Infrared Physics & Technology*, vol. 85, pp. 246-250, 2017.
- [13] W. Dobbelaere, J. De Broek, C. Bruynseraede, R. Mertens and G. Borghs, "InAsSb light emitting diodes and their applications to infra-red gas sensors," *Electronics Letters*, vol. 29, no. 10, 1993.
- [14] Y. Mao and A. Krier, "InAsSb p-n junction light emitting diodes grown by liquid phase epitaxy," *Journal of Physics and Chemistry of Solids*, vol. 56, no. 5, pp. 759-766, 1995.
- [15] Y. Mao and A. Krier, "Efficient 4.2um light emitting diodes for detecting CO₂ at room temperature," *Electronics Letters*, vol. 32, no. 5, 1996.
- [16] A. A. Popov, M. V. Stepanov, V. V. Sherstnev and Y. P. Yakovlev, "InAsSb light-emitting diodes for the detection of CO₂ ($\lambda = 4.3\mu\text{m}$)," *Technical Physics Letters*, vol. 24, no. 8, 1998.
- [17] V. K. Malyutenko, A. V. Zinovchuk and O. Y. Malyutenko, "Bandgap dependence of current crowding effect in 3-5um InAsSb/InAs planar light emitting devices," *Semiconductor Science and Technology*, vol. 23, no. 8, 2008.
- [18] R. M. Biefeld, A. A. Allerman, S. R. Kurtz, et. al., "Recent advances in mid-infrared (3-6um) emitters," *Mat. Sci. Eng. B*, vol. 51, 1998.
- [19] H. R. Hardaway, J. Heber, P. Moeck, M. J. Pullin, T. Stradling, P. J. P. Tang and C. C. Phillips, "Optical studies of InAs/In(As,Sb) single quantum well (SQW) and strained-layer superlattice (SLS) LEDs for the mid-infrared (MIR) region," *SPIE Proceedings - Light emitting diodes: research, manufacturing and applications III*, vol. 3621, 1999.
- [20] B. Grietens, S. Nemeth, C. Van Hoof, P. Van Daele and G. Borghs, "Growth and characterisation of mid-IR InAs_{0.9}Sb_{0.1}/InAs strained multiple quantum well light emitting diodes grown on InAs substrates," *IEEE Proceedings Optoelectronics*, vol. 144, no. 5, 1997.
- [21] A. Krier, M. Stone, Q. D. Zhuang, P. W. Liu, G. Tsai and H. H. Lin, "Mid-infrared electroluminescence at room temperature from InAsSb multi-quantum-well light-emitting diodes," *Applied Physics Letters*, vol. 89, no. 9, 2006.
- [22] M. J. Pullin, H. R. Hardaway, J. D. Heber, C. C. Phillips, W. T. Yuen and R. A. Stradling, "Room-temperature InAsSb strained-layer superlattice light-emitting diodes at 4.2um with AlSb barriers for improved carrier confinement," *Applied Physics Letters*, vol. 74, no. 16, 1999.
- [23] J. A. Keen, D. Lane, M. Kesaria, A. R. J. Marshall and A. Krier, "InAs/InAsSb type-II strained-layer superlattices for mid-infrared LEDs," *Journal of Physics D: Applied Physics*, vol. 51, no. 7, p. 075103, 2018.
- [24] J. W. Matthews and A. E. Blakeslee, "Defects in epitaxial multilayers. I. misfit dislocations," *Journal of Crystal Growth*, vol. 27, no. 118, 1974.
- [25] K. Muraki, S. Fukatsu and Y. Shiraki, "Surface segregation of In atoms during molecular beam epitaxy and its influence on the energy levels in InGaAs/GaAs quantum wells," *Applied Physics Letters*, vol. 61, no. 5, 1992.
- [26] S. Birner, T. Zibold, T. Andlauer, T. Kubis, M. Sabathil, A. Trellakis and P. Vogl, "Nextnano: general purpose 3D simulations," *IEEE Transactions on Electron Devices*, vol. 54, no. 9, 2007.
- [27] P. J. Carrington, V. A. Solov'ev, Q. Zhuang, A. Krier and S. V. Ivanov, *Applied Physics Letters*, vol. 93, 2008.

Highlights

- InAs/InAsSb low-antimony type-II superlattice structures grown by MBE
- Fabrication of LED devices featuring active region of InAs/InAsSb SLS structure
- Mid-infrared electroluminescence over 7-300 K temperature range, with spectra coinciding with the CO₂ absorption peak at 4.2 μm
- Comparison of electroluminescence and photoluminescence spectra at low temperature (7K/4K) and at room temperature (300K).